Rapid-turnaround characterization methods for MRAM development

D. W. Abraham
P. L. Trouilloud
D. C. Worledge

Magnetic random access memory (MRAM) technology, based on the use of magnetic tunnel junctions (MTJs), holds the promise of improving on the capabilities of existing charge-based memories by offering the combination of nonvolatility, speed, and density in a single technology. In this paper we review rapid-turnaround methods which have been developed or applied in new ways to characterize MRAM chips at various stages during processing, with particular emphasis on the MTJs. The methods include current-in-plane tunneling (CIPT), Kerr magnetometry, vibrating sample magnetometry (VSM), and conducting atomic force microscopy (CAFM). Use of the methods has enabled rapid learning with respect to the materials used for the MTJs, as well as tuning of the MTJ geometry in terms of size and shape and of the patterning methods employed. Examples of the use of each of the methods are presented along with interpretation of the data via critical operating parameters.

Introduction

The basic MTJ contains one or two pinned (or reference) layers, an intervening tunnel barrier, and one or two free (or storage) layers. Typically, a pinned layer consists of a ferromagnetic film deposited in intimate contact with an antiferromagnetic film. These two films act to establish a stable magnetic orientation for magnetic fields up to several hundred oersteds. A free layer consists of either a simple thin film of ferromagnetic material (for Stoner–Wohlfarth switching)[1] [1–3] or a multilayer structure comprising magnetic and spacer layers (for toggle switching, also referred to as rotational switching) [4, 5]. The tunnel barrier is formed by oxidation of a thin metal film (usually an Al or Mg film) which is grown between the pinned and free layers. In addition to the magnetically active layers, there are also seed, cap, and growth layers intended to act as thermal diffusion barriers as well as to promote high-quality film growth of subsequent layers. A more detailed description of the operation of this device is presented in a companion paper in this issue [6].

In the course of MRAM chip fabrication, many measurement methods have been developed or adapted in order to provide early feedback about the eventual properties of the chip as well as to monitor changes in properties due to the processing itself. The measurement techniques reviewed in this paper can be divided into two groups, depending on whether they are used to measure the properties of the blanket films (via Kerr, VSM, and CIPT) or patterned MTJs (via Kerr and CAFM). Assessment by Kerr magnetometry and vibrating sample magnetometry (VSM) reveals important information about the effectiveness of relevant magnetic properties such as pinning, magnetic skew, and Néel coupling. In the blanket film stage, it is also possible to evaluate the magnetization polarization, tunnel barrier resistance, layer smoothness, and so on through the use of a technique developed at IBM designated as current-in-plane tunneling (CIPT) [7, 8].

The fully integrated MRAM chip contains not only magnetic storage devices but also the peripheral wiring and CMOS elements which permit read/write operation on-chip. However, much of the critical characterization work for MRAM development can be done on patterned MTJs of an MRAM chip without the need to fabricate fully connected structures. We have prepared photolithography masks for preparation of arrays of MTJs which permit direct measurement of magnetic switching using highly sensitive Kerr magnetometry. In addition, alternating gradient (AGM) and SQUID magnetometers have been used in this role, providing the

---

[1] Simon Middelhoek, University of Amsterdam, private communication, 1961.

0018-8646/06/$5.00 © 2006 IBM

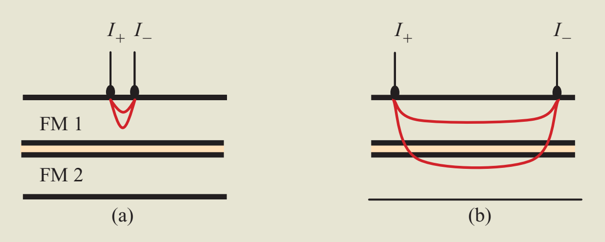

Figure 1

Schematic of the current flow in an MTJ to be tested via CIPT as a function of probe spacing. Here, FM 1 and FM 2 refer to top and bottom ferromagnetic thin films, respectively, separated by a tunnel barrier. If the current probes are placed too close (a), all of the current flows through the top layer. The MR cannot be measured because the current does not sample the barrier. If the current probes are placed too far apart (b), the current flows in parallel through both top and bottom layers, as if the barrier were not present. In this case, the MR cannot be measured because the contribution by the barrier to the total measured resistance is too small.

advantage of calibrated measurement of sample moment but with increased measurement time and reduced flexibility. Such array measurements of switching have proven to be invaluable in revealing the switching properties of arrays of MTJs, and in particular have been shown to reveal the sources of spreads in these properties which can serve as MRAM yield limiters. In addition, by leaving a ground plane connecting the lower portions of all of the MTJs, electrical measurements can be made on individual MTJs using a conducting atomic force microscope (CAFM) as a precise electrical probe.

Blanket film characterization methods

The initial task facing development of an MRAM cell is the development of the magnetic film stack. Starting in the unpatterned state, the films of the stack should exhibit good thermal stability, high magnetoresistance (MR), good pinning, and low Néel coupling between the pinned and free layers. By measuring these properties directly after deposition and annealing, rather than after patterning, a decrease in turnaround time amounting to a factor of 10 or more can be achieved. Thus, accurate methods for characterization at this stage are critical for rapid learning. Three tools are used at this stage: CIPT, which measures the sheet film resistance–area product (RA) of the tunnel barrier as well as the MR; Kerr magnetometry, which provides an immediate look at the magnetization hysteresis loops; and vibrating sample magnetometry, which complements Kerr measurements by providing a calibrated measure of magnetization for each of the constitutive layers in the stack. We now describe these methods.

Current-in-plane tunneling (CIPT)

It is a simple experimental fact that the more processing an MRAM wafer experiences, the more likely it is that its MTJs will be degraded. This makes it difficult to evaluate MTJ fabrication without influence from subsequent fabrication steps. Furthermore, since a well-established and reliable processing route is often tuned to the particular materials used in the MTJ stack, it has limited use in experimentation with new materials. In addition, it is useful to be able to characterize MTJ fabrication rapidly in order to permit faster development of new materials and deposition processes, and also to facilitate regular and timely monitoring of a "standard" MTJ wafer process. All of these objectives can be met by using CIPT [7, 8].

CIPT involves extracting the MR and RA of an unpatterned (and unprocessed) wafer by making a series of four-point-probe resistance measurements on the surface of the wafer. The wafer is pre-set to the low- and high-resistance states by applying an external magnetic field corresponding to the free and pinned layers being parallel or anti-parallel to one another. Values of RA are measured for each of these configurations, and MR is defined as $MR = 100(RA_{\text{high}} - RA_{\text{low}})/RA_{\text{low}}$. Each resistance measurement is carried out at a different mean probe spacing, typically in the range of 1.5 μm to 20 μm. In this range, the current flows partly through the top metal layer and partly through the tunnel barrier into the bottom metal layer, permitting measurement of the properties of the tunnel barrier. At relatively small probe spacings, the current is confined to the top metal layer, since the barrier resistance (averaged over the area between the tightly spaced probes) is large compared to the sheet resistance of the top metal film between the same two probes [see **Figure 1(a)**]. At relatively large probe spacings, the current easily traverses the barrier (which has a very low resistance over this large area), and spreads out over both the bottom and top metal layers like two resistors in parallel, as if the barrier were not there [**Figure 1(b)**]. Therefore, the MR cannot be measured at such large probe spacings, since the contribution by the barrier to the total resistance is so small. However, at some intermediate probe spacing, the current can flow through both top and bottom layers and the barrier can still contribute a significant fraction of the total resistance, so that the MR can be measured. From dimensional analysis, one can guess that this length scale is

$$\lambda = \sqrt{\frac{RA}{R_T + R_B}}, \tag{1}$$

where R_T and R_B are the resistances per square of the top and bottom layers. When probes are placed on the

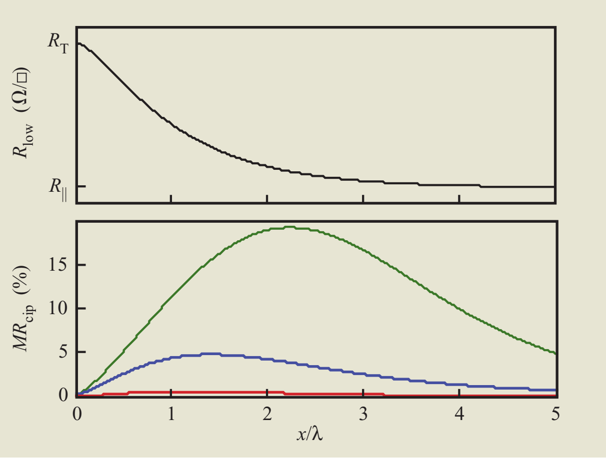

Figure 2

Calculated resistance per square and MR_{cip} as a function of probe spacing. At small probe spacings the resistance per square is given by the top layer; at large spacings it is given by the parallel combination of top and bottom layers, $R_{||} = R_T R_B/(R_T + R_B)$, as expected from Figure 1. The MR_{cip} depends on both λ and the ratio R_T/R_B. The green, blue and red traces correspond to $R_T/R_B = 10$, 1, and 0.1, respectively. Adapted from [8], with permission.

surface of the wafer with a spacing near λ, the measured resistance is between that of the top layer and that of the parallel combination of the top and bottom layers, and the MR can be measured.

In practice the measurements are carried out at a series of different probe spacings, ideally spanning a range which includes λ, and the data is then fitted to a theoretical prediction [8] for resistance R, given by

$$R = \frac{V}{I} = \frac{R_T R_B}{R_T + R_B}\frac{1}{2\pi}\left\{\frac{R_T}{R_B}\left[K_0\left(\frac{a}{\lambda}\right) + K_0\left(\frac{c}{\lambda}\right) - K_0\left(\frac{a+b}{\lambda}\right) - K_0\left(\frac{b+c}{\lambda}\right)\right] + \ln\left[\frac{(a+b)(b+c)}{ac}\right]\right\}, \qquad (2)$$

where the distance between I_+ and V_+ is a, V_+ and V_- is b, and V_- and I_- is c. Here K_0 is the modified Bessel function of the second kind of order zero. The measured magnetoresistance, MR_{cip}, can be calculated from $MR_{cip} = 100(R_{high} - R_{low}) / R_{low}$, where R_{high} and R_{low} are calculated from Equations (1) and (2) using RA_{high} and RA_{low}, respectively. In **Figure 2**, Equation (2) is plotted for R_{low}, showing how the resistance per square starts out at R_T at low probe spacing and then transitions, around $x = \lambda$, to $R_{||}$, the parallel combination of R_T and R_B at large probe spacings. Figure 2 also shows MR_{cip} as a function of probe spacing, for several different values of R_T/R_B. Note that when R_T is significantly smaller than R_B, very little MR_{cip} is measured, because the top layer effectively shorts out the measurement and very little current travels through the barrier.

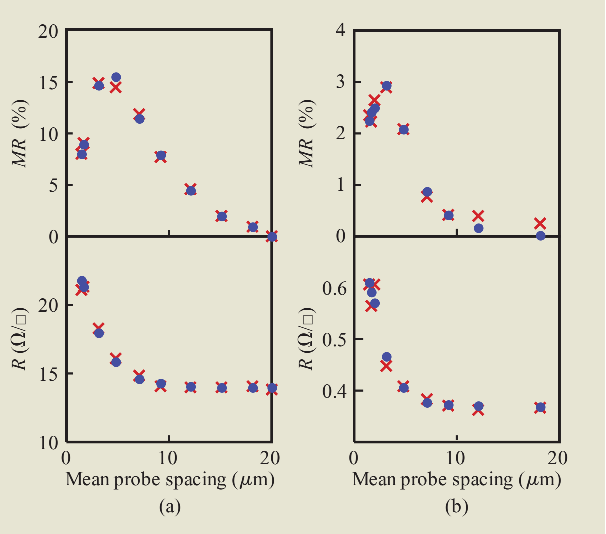

(a)

(b)

Figure 3

Examples of CIPT data for two different samples: (a) Data obtained from a sample with an MgO tunnel barrier. The fit gives $MR = 169\%$, $RA = 370$ Ω-μm², $R_T = 25.6$ Ω/□, and $R_B = 30.6$ Ω/□. (b) Measurement performed on a low-RA sample. Here, the fit gives $RA = 5.78$ Ω-μm², $MR = 16.5\%$, $R_T = 0.79$ Ω/□, and $R_B = 0.69$ Ω/□.

Figure 3(a) shows an example of the data obtained in our laboratory using a commercial CIPT tool [9]. The tool uses a twelve-point probe micromachined from Si/SiO$_2$ and metallized with Au. A good probe typically lasts for about 100 touchdowns. The twelve cantilevers each extend the same distance from the substrate, so that they contact the sample on 12 points in a straight line. The inner four probes are spaced 1.5 μm apart tip to tip, and the outer probes on both sides are placed at successively larger probe spacings, with the last probes spaced about 10 μm tip to tip. This choice of probe spacing allows tunnel barrier RA values ranging from 1 to 10^5 Ω-μm² to be measured (depending on the conductivity of the top and bottom metal films employed). A multiplexer permits measurement with any four of the twelve probes, which are irregularly spaced from 1.5 μm to 10 μm apart; this allows for mean probe spacings varying from 1.5 μm to 18 μm. A magnetic field from a toroidal electromagnet switches the resistance back and forth between the high and low states, while a lock-in amplifier is used to measure the resistance. By switching the field many times, good statistics can be obtained on the measured resistance and MR_{cip}. In Figure 3, the x symbols represent the data and the circles are the fit to Equation (2). To add to the data at large probe spacings, a measurement of the resistance per square was made using a macroscopic four-point probe tool, with spacing = 1 mm (the MR was assumed to be zero at this large spacing); this data is plotted at a probe spacing $x = 20\ \mu\text{m}$. The measured resistance and MR_{cip} data are then simultaneously fit to the theory by adjusting the four parameters MR, RA, R_T, and R_B. For this sample with an MgO barrier, the fit gives $MR = 169\%$, $RA = 370\ \Omega\text{-}\mu\text{m}^2$, $R_T = 25.6\ \Omega/\square$, and $R_B = 30.6\ \Omega/\square$. Data obtained at smaller probe spacings are usually noisier because of positional errors in the probes. A method of correcting for these positional errors by performing a second measurement with the I_+ and V_+ leads interchanged and then taking a linear combination of these two measurements has been discussed elsewhere [10].

Because the length scale λ involves R_T and R_B, CIPT can be used to measure samples with much lower RA by using smaller values of R_T and R_B to maintain λ around 1.5 μm or higher. **Figure 3(b)** shows an example with $RA = 5.78\ \Omega\text{-}\mu\text{m}^2$, $R_T = 0.79\ \Omega/\square$, and $R_B = 0.69\ \Omega/\square$. If this sample had values of R_T and R_B as large as the sample in Figure 4(a) (shown later), no useful CIPT data would have been obtainable down to a mean probe spacing of 1.5 μm, and a different probe with smaller probe spacing would have been needed. However, since this sample had a much smaller R_T and R_B (less than 1 $\Omega/\square$), λ was large enough to allow useful data to be obtained.

CIPT has been used to measure more than 3,500 samples in our laboratory, including samples for tunnel barrier optimization, new free-layer materials, thermal stability studies, within-wafer uniformity, wafer-to-wafer uniformity, and long-term process stability. The measurement time of a few minutes per sample facilitates rapid materials development. (By comparison, a few days or weeks are usually required for sample fabrication.) In addition, it is useful to be able to deconvolve the deposition process from the patterning processes, thus allowing development of MTJ stacks using new materials without having to simultaneously develop new patterning processes.

Kerr magnetometry for sheet films

Just as CIPT has been shown useful in characterization of the electrical transport properties of an intact MRAM film stack, Kerr magnetometry has proven invaluable in providing an early readout of the magnetic properties of freshly deposited MTJ films. Both methods taken in tandem provide a clear view of the initial properties of the magnetic stack. By establishing a baseline measurement of these properties directly after film preparation, it is possible to understand the effects of process steps involved in fabricating the MTJ. Many fundamental magnetic parameters can be measured, including film coercivity and loop squareness, anisotropy (magnitude, orientation angle, and dispersion), pinning strength and orientation, and interlayer coupling (due to exchange or Néel coupling). Kerr magnetometry allows for rapid progress by quickly cycling between film deposition and Kerr characterization. Subtle changes in stack parameters due to various controlled changes can be quantified quickly and, if desired, investigated for final MTJ properties by continuing fabrication. Typically, film thickness changes and changes in deposition parameters (source power or deposition rates, material composition, etc.) can be adjusted while providing nearly immediate feedback as to the resultant magnetic properties. The stack can also be studied by measurement after reset annealing, permitting tuning of magnetic properties such as anisotropy and interlayer coupling, and optimization of the maximum temperature to which the stack can be exposed before spin-polarized tunneling starts to degrade.

Longitudinal Kerr magnetometry measures the rotation of the polarization of light reflected from the surface of a magnetic material under study as a function of applied magnetic field. The Kerr signal is proportional to the magnetic moment of the sample under test, but a fundamental calibration constant giving a quantitative measure of sample moment per amount of polarization rotation is not available. Nonetheless, for a given sample or set of similar samples, the Kerr signal is proportional to the sample magnetization parallel to the optical beam, with the same calibration constant for all samples within the series. For the measurements of sheet film magnetic samples, we have used a single-field-axis Kerr magnetometer (ADE Technologies, Westwood, MA). The sample can be positioned precisely at desired locations on a 200-mm-diameter wafer and can be rotated so that the field and measurement axis can be oriented at any angle with respect to the magnetic easy axis. Typically, samples are measured after deposition and annealing and the critical parameters mentioned above are tabulated.

Figure 4 shows typical data for a Stoner–Wohlfarth stack measured before patterning. In this stack, shown schematically in Figure 4(a), the free layer consists of a single ferromagnetic thin film, and the pinned layer comprises a pair of exchange-coupled ferromagnetic thin films deposited onto an antiferromagnetic layer. The pinned layer is designed so that, once patterned in MTJs, the net dipole field from the pinned layer acting on the free layer compensates for the small Néel contribution. In addition, pinning the bottom ferromagnetic film to the antiferromagnet should allow the magnetic orientation of the pinned layers to remain fixed in the modest fields used during device switching. The data is taken both along the easy axis (defined as the direction of magnetic field during reset anneal done immediately after film deposition) and along the hard axis (defined as perpendicular to the film easy axis). At low fields, the easy-axis data in Figure 4(b) shows a square loop with a low value of coercivity of 4.6 Oe, indicating that the free layer is of high quality and is nearly independent of the pinned layer. Very little Néel coupling is observed between the pinned and free layers, as seen in an offset of the EA loop center of 0.9 Oe. At higher fields [Figure 4(c)], the reversal of the pinned layer is seen. From the measured values of H_+ and H_-, defined as the high-field limits of the observed flat plateau, it is possible to extract both the pinning field and the interlayer exchange coupling J according to the following expressions:

$$H_\mathrm{p} = |H_-| - H_+ ;$$

$$J/M_\mathrm{s} t = \frac{|H_-| H_+}{|H_-| - H_+} .$$

For the sample shown here, $J = 1.1$ erg/cm^2 and $H_\mathrm{p} = 3{,}200$ Oe. For this case, $M_\mathrm{s} = 1{,}500$ emu/cm^3 and $t = 3.5$ nm, as determined by VSM measurements (see next section) of similar films and known film deposition rates. Hard-axis data is shown in Figure 4(d). At low field ranges the free-layer response dominates, and the effective anisotropy H_k can be inferred from the extrapolation of the low-field data to saturation. For this sample, $H_\mathrm{k} = 23$ Oe. The degree of anisotropy dispersion could be obtained from this data, particularly with respect to loop opening and the appearance of discrete jumps in the moment vs. field. For the case shown here, very little dispersion was observed. By repeating these measurements at a grid of points across the wafer, it is possible to form a map of these properties across macroscopic distances and thus obtain the anisotropy skew, a measure of the rotation of the anisotropy axis over the wafer (the analog of the microscopic variability referred to above as dispersion).

Quantitative interpretation of the magnitude of the Kerr rotation signal in terms of the orientation of the magnetic layers in multilayer samples is complicated by the layer and depth dependence of the optical signal, and by the dependence of this signal on material characteristics. The introduction of empirical fitting parameters to account for the signals from different layers (for example, for understanding the behavior of rotational free layers) has been successfully used to explain the observed trends and details of the measured hysteresis loops.

Vibrating sample magnetometry (VSM)

The Kerr magnetometer discussed above provides rapid feedback with accurate characterization of critical magnetic behavior as a function of magnetic field. For certain applications it is important to have a quantitative measure of the moments of the magnetic layers of a stack. We have used a variety of methods to this end, but have predominantly used the vibrating sample magnetometer, or VSM (ADE Technologies, Westwood, MA). The noise floor of our VSM (roughly one micro-emu) corresponds to angstrom level sensitivity in layer thickness. The VSM operates by vibrating the sample and thereby inducing a voltage in a pair of nearby pickup coils. The coils are situated on the pole pieces of a magnet capable of providing a magnetic field of up to 2 T. In another mode, the sample can be placed in a bottle oven fitted with a pair of orthogonal pickup coils so that both in- and out-of-plane components of moment can be measured simultaneously. The oven permits direct measurements of the moment vs. the temperature for studies of the thermal stability of the MTJ stack materials.

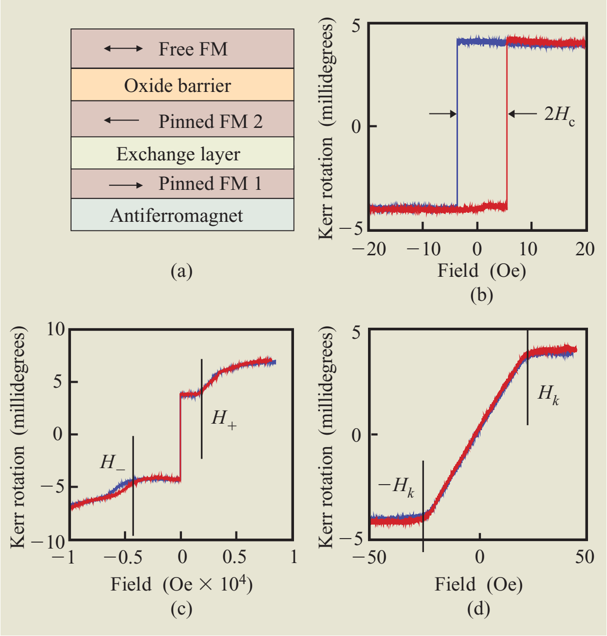

Figure 4

(a) Typical data for a Stoner–Wohlfarth stack. (a) Kerr easy-axis (EA) data taken at low field, showing the excellent low Néel offset and sharp hysteresis loop. (c) High-field EA Kerr magnetometry data showing the relative motion of the magnetization in the two ferromagnetic films, permitting direct measurement of pinning and interlayer coupling. (d) Hard-axis data revealing the film anisotropy.

Typically, VSM measurements require the samples to be broken into small pieces and fixed to the VSM probe; the time required for data acquisition is several minutes per scan. However, this lack of flexibility is warranted in cases requiring calibrated measurements. For example,

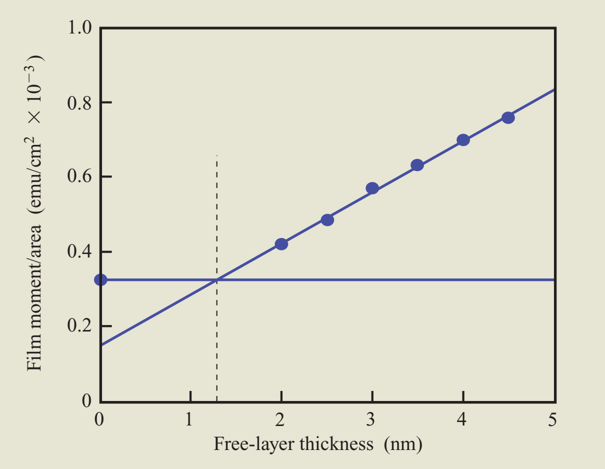

Figure 5

Illustrative VSM results for film moment/area vs. free-layer thickness. VSM can be used to provide a direct measure of the magnetization/volume and of the "dead" layer associated with film growth on various substrates (indicated by the dashed vertical line).

in samples containing magnetic layers with balanced and opposing moments, the direct measure of the moments of each layer allows a rapid tuning of the magnetic stack. In addition, the balance condition for the freshly prepared sheet film stack can be compared with that determined for the patterned MTJ. This information constitutes important feedback regarding the patterning process, for example providing information about structural imperfections such as tapered profiles and information about moment reduction from chemical effects which might affect one layer preferentially.

Another example of the usefulness of VSM for MTJ development is in the direct measurement of sample moment vs. layer thickness. The surface upon which the magnetic material is grown often has a retarding effect on the development of magnetic moment for the first several monolayers of growth, creating a magnetically "dead" layer. **Figure 5** shows the moment/area for a series of samples with increasing free-layer thickness starting with the absence of a free layer, all grown on a standard synthetic antiferromagnetic (SAF) pinned layer capped by an AlO tunnel barrier. (The SAF consists of two thin ferromagnetic films separated by an exchange-coupling layer, typically a Ru layer. The combination acts as a zero-moment single layer for fields below that which is able to disturb the anti-parallel alignment of the two coupled ferromagnetic films.) The slope of the moment/area vs. free-layer thickness (discounting the zero thickness sample) gives the free-layer magnetization m_s, equal here to 1,375 emu/cc. The intersection of this data with the value corresponding to the absence of a free layer occurs at 1.28 nm. This corresponds to a dead layer and must be accounted for in evaluating the stability of MTJs against thermally activated switching events, the balancing of rotational free layers, and the thermal degradation of the magnetic properties of an MTJ device.

Patterned sample characterization

The magnetic films discussed above are the first step in the process of creating an MTJ. In order to complete the process, as mentioned, the film stack must be masked and material removed in order to leave an island of the desired shape protruding from a base layer. Characterization of the MTJ can wait for final integration, at which point the chip can be interrogated by traditional probe testers. However, this process requires significant additional investment in time to complete (often much more than that required to fabricate patterned MTJs) and, in addition, the final product can fail or degrade during these subsequent steps. Hence, early characterization methods that can measure electrical and magnetic behavior of the MTJ device immediately after patterning are critical in providing rapid feedback as well as isolating the tunnel junction patterning method which is so central to the process of fabricating an MRAM chip. We have used CAFM and Kerr magnetometry to meet this need.

Conducting atomic force microscopy (CAFM)

CAFM can be used to test MTJs during processing, before the formation of their lithographically defined top and bottom contacts. A metallized atomic force microscope tip is used to contact the top surface of an MTJ after etching [11–13]. The technique can be used to measure *MR*, *RA*, H_c, H_s, hysteresis loops, astroids, *I–V* curves, breakdown voltage, and the bias dependence of the MR and RA. The MTJs can be probed directly after patterning, and also after subsequent processing steps such as dielectric deposition and annealing. This rapid-turnaround technique permits measurements to be made in minutes that would otherwise take additional days or weeks of processing, thus speeding up process development. In addition, it allows the measurement of MTJs during processing, which helps to isolate effects that may occur after processing steps; this data cannot be obtained with traditional techniques.

The CAFM technique requires the sample to have a conducting cap. It is the conductance of the surface of the cap that is important here: Most metals are not suitable, since they oxidize to insulators on the top 1 nm or so of the cap. We have typically used two different materials for the cap: Ru and TiN. A 3–10-nm-thick layer of Ru works particularly well as the cap, since RuO_2 is a good conductor, and Ru is readily available in the deposition chamber because it is used as the spacer for the AP pinned layer [**Figure 6(a)**]. The samples are patterned as shown in **Figure 6(b)**. First, e-beam or optical resist is used to mask off a variety of MTJ shapes and sizes. Then the MTJs are etched with the process under study—for example, RIE, ion milling, or wet etching. This is done in order to leave behind a continuous underlying metal layer connecting all of the MTJs. This layer is used as the current return path. **Figure 6(c)** is a schematic diagram of the measurement. An AFM tip coated with sputtered PtIr is first used to image the sample in order to locate the MTJs; this can be done in either tapping or contact mode. Then the tip is centered on one MTJ (and if tapping mode is used, lowered into contact). An external source meter is used to measure the resistance as a function of applied field, using a toroidal electromagnet placed in the AFM chuck. This method is capable of measuring MTJs as small as 200 nm × 200 nm. Large devices can be measured as well, with typical CAFM contact resistances of 30 Ω eventually limiting the measurement accuracy. Repeated measurements can be made on a single MTJ without any apparent degradation in MTJ performance or properties, indicating that contact damage is negligible.

Figure 7 shows typical data obtained via CAFM. The resistance vs. easy-axis field is plotted for a Stoner–Wohlfarth tunnel junction having an MgO barrier [14]. The coercivity and loop shift can easily be calcuated from the transitions in the hysteresis loop. The RA and MR can be calculated from the high- and low-resistance levels, using the nominal area. These are shown in the inset for nine nominally identical MTJs. By applying a hard-axis field while sweeping the easy-axis field, the entire switching astroid can be mapped out.

The CAFM method can also be extended for use with rotational, or toggle [5, 15] MTJ samples. **Figure 8** shows an example of data for a typical sample. The field trajectories are shown in Figure 8(a): The swept-loop field is shown in red, illustrating a field path along the easy axis of the device, while the toggle measurements, shown in orange and green, are performed using square paths of increasing field size. Both positive and negative square paths are typically used, with the expectation that the device will toggle once the field exceeds the spin-flop field and will cease toggling once the saturation field is achieved. Data for swept-field and toggle switching are shown in Figures 8(b) and 8(c), respectively. In the swept data, a central hysteretic region is formed with both high- and low-resistance states sampled, depending on the sign of the field as the field passes through the direct-write boundary. Also observed in the swept loops are the toggle and direct-write fields, as indicated. These fields can be seen in the toggle measurements as

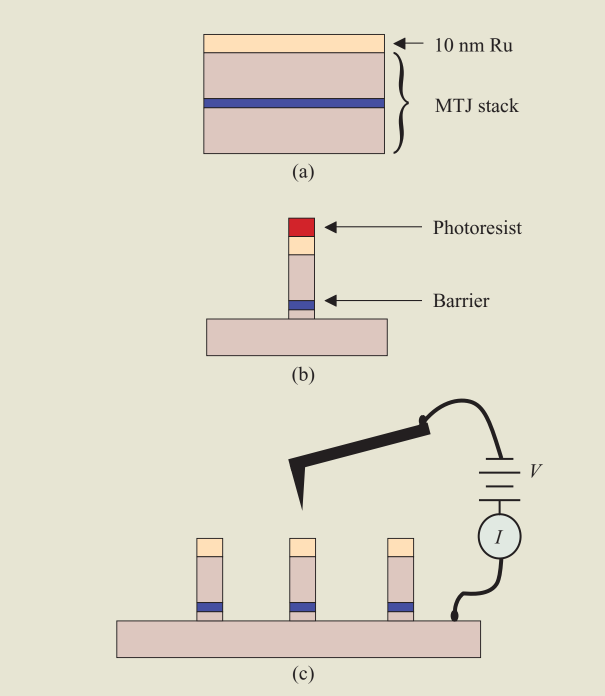

Figure 6

Schematic of the CAFM technique. The sample (a) must have a conducting cap, for example, a thin layer of Ru. Lithography and etching define the MTJs (b), leaving behind a common bottom electrode. A metal-coated AFM tip is used to contact the top of an MTJ (c) in order to measure the current I flowing under a voltage bias V.

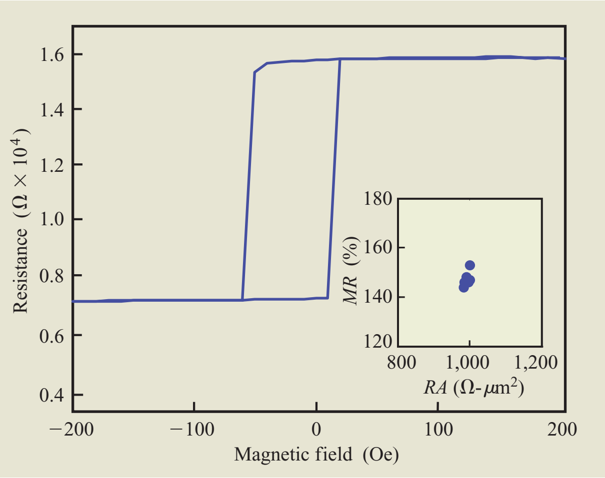

Figure 7

Example of a swept hysteresis loop obtained via CAFM by measuring the resistance of a 300-nm × 600-nm MTJ as a function of applied easy-axis field. The inset shows a summary of nine such measurements on nominally identical MTJs.

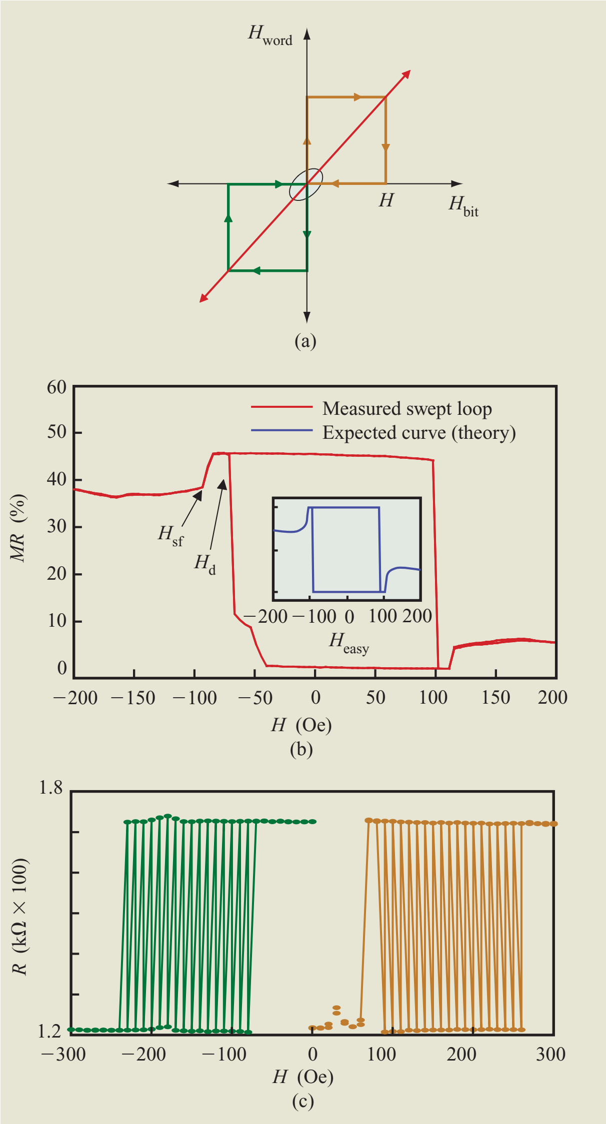

Figure 8

CAFM data taken on a rotational-stack MTJ. The field paths shown in (a) correspond to swept loops with field applied along the easy axis of the MTJ, while the orange and green traces show a single toggle pair of paths used to test for switching. Swept-loop data in (b) compares favorably with the model shown in the inset and reveals key features such as the direct-write field and the spin-flop field. Toggle data directly measures the MTJ by repeatedly switching the MTJ between the two stable states (c), providing another, more stringent test of cell operation in a rapid-feedback measurement.

well [Figure 8(c)] as a single transition of the resistance without toggling (at the direct-write field) followed by the onset of toggling at a slightly higher field. The values of magnetoresistance seen in the swept and toggle data are the same, as expected.

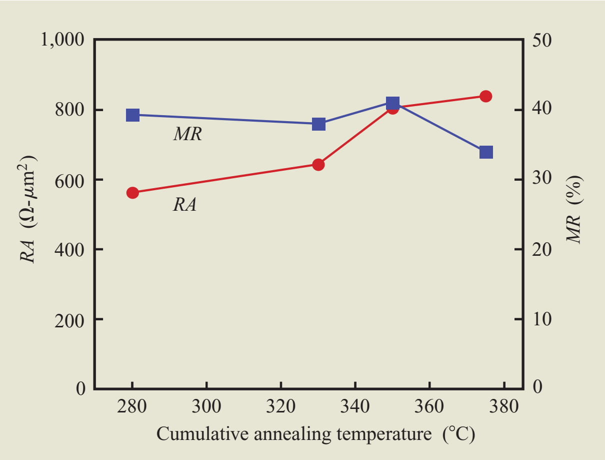

Figure 9

Example of the results of thermal stability measurement on encapsulated MTJs. Each point pertains to an average of five MTJs after cumulative annealing of one hour at each temperature.

The Stoner–Wohlfarth switching data shown in Figure 7 was measured at a dc bias of 10 mV. By applying different amounts of bias when obtaining the hysteresis loop, the bias dependence of R and MR can be measured, providing direct measurement of parameters such as V_{50}, the bias at which the MR drops by 50%. By fixing the field at zero and measuring the resistance as the bias is changed, the *I–V* curve can be obtained. Furthermore, by applying ever-larger bias until the MTJ is destroyed, the breakdown voltage of the tunnel barrier can be measured.

One of the advantages of using the CAFM technique is that samples can be measured at multiple steps throughout the fabrication process. This allows each process step to be isolated and checked. For example, samples can be etched and then measured, followed by dielectric encapsulation, and then measured again. In this case the MTJ must be exposed after dielectric deposition. This can be done either by polishing back the dielectric or by lifting off a resist mask in acetone. After dielectric encapsulation, measurement can continue (for example, after successive annealing, as shown in **Figure 9**). This is done in order to evaluate the thermal stability of the MTJ stack materials (which could be done at the sheet film level using CIPT) and also the interaction of the MTJ stack with various etching chemistries and dielectrics.

CAFM is a useful technique because of its relatively fast turnaround time and because it permits sample measurement to be checked after individual process steps. The method is particularly useful for etching process development, studying thermal stability, and evaluating the use of alternate materials.

Kerr magnetometry for patterned films

As is the case for sheet films, the Kerr magnetometer is the first choice for the magnetic characterization of patterned MTJ arrays. Similar considerations regarding the sensitivity of the amplitude of the signal to the specifics of the magnetic layer under consideration apply in the analysis of the data obtained for patterned arrays as well. One concern that immediately arises is that the signal strength is reduced roughly by the fill factor of the MTJ array: Typically this is in the range of 5%, corresponding to a twentyfold drop in signal. A second concern is the effect on the signal strength of the two-dimensional diffraction grating formed by the MTJ array.

In contrast to CAFM or CIPT, the sample need not contain reference layers. Kerr measurements can be applied to simplified structures such as free-layer-only stacks. This freedom permits study of the effects of the pinned layer vs. the intrinsic nature of the free layer in a patterned MTJ. Thus, imperfections in the MTJ can be dissected by intentionally fabricating structures which omit portions of the structure.

In measuring the switching characteristics of Stoner–Wohlfarth MTJ arrays, the magnetic field is usually applied along the device easy axis. The observed hysteresis loop is not perfectly square, and the rounding observed can be related to the distribution of switching fields in the array. This distribution can be characterized by a single parameter which we have termed the array quality factor (AQF), defined as the ratio of the switching field to the standard deviation of the switching field. AQF is a useful parameter because it determines the eventual yield of an MRAM chip. For example, our 16-megabit design [3] requires that $AQF > 20$ in order to experience on average less than one error per decade. Rather than measuring yield in the usual manner (by measuring a fully fabricated chip in parametric or functional test), it is instead possible to perform rapid-turnaround-time experiments using Kerr magnetometry. For example, **Figure 10** shows the effect of aspect ratio of the patterned shape on the AQF. The effect of increasing aspect ratio is twofold: First, the switching field rises dramatically; second, the standard deviation drops, as seen by the narrowing of the switching field distribution for increasing aspect ratio. Thus, Kerr data shows that the AQF rises dramatically with aspect ratio, a result confirmed in subsequent electrical measurements on completed chips. Selection of a particular sample size and shape for use in an MRAM chip is based on the surpassing of a minimum value of the AQF while doing so with a switching field that can be reached under the currents available to flow in the word lines and bit lines on chip.

Rotationally (or toggle) switched devices can also be characterized by Kerr magnetometry, although the concepts governing optimal operation are somewhat different than in the Stoner–Wohlfarth case. The first requirement is that the two magnetic layers in the free layer must be of equal moment. As already discussed, sheet film stacks are designed so that the moments/area of each layer are equal. However, subtle differences arise during processing so that additional tuning of the layer thicknesses is required to achieve final balance after the MTJ is formed. **Figure 11** shows the effect of increasing the thickness of the upper layer. Several features can be used to pinpoint the best balance condition: First, the thicker film points in the direction of the applied field as the field approaches zero. Thus, at balance the positive and negative branches of the hysteresis loop exchange with one another: For the series with the top film thinner than the bottom (corresponding to the two leftmost graphs), the red trace is on top near zero field, while for the opposite case (the two rightmost graphs) the traces reverse and the blue data is on top. Second, the shape of the curve changes in agreement with the predictions of the single-domain model, essentially reflecting the increasing separation of direct-write and spin-flop fields with increasing imbalance. Finally, the toggle field can be extracted by fitting the data (see **Figure 12**), and is expected to be at a minimum for the balanced stack. As described previously, CAFM data can also be analyzed to quantitatively extract H_{d} and H_{sf} in order to determine the best-balance condition for the MTJ stack (Figure 8).

For the understanding of patterned structures, particularly for rotationally switched samples, it can be necessary to measure the magnetization as the field follows an arbitrary trajectory. We have used a double-axis Kerr magnetometer system from ADE Technologies which has the capability of applying fields simultaneously in two orthogonal axes. It can thus apply an arbitrary field trajectory in the xy plane. The tool also simultaneously measures the longitudinal Kerr effect signal along both x and y in-plane axes. As in the single-axis Kerr magnetometer system described previously, the measurement is an average of the response of all of the MTJs sampled by the laser spot of the system. In the double-axis Kerr magnetometer system, two laser spots are carefully aligned to sample the same area, which is less than 200 μm in diameter. A significant advantage of the double-axis tool is that the detection axes can also be selected arbitrarily and independently of the applied field directions. The MTJs can be prepared in a known state by applying an initialization sequence, and their response to write sequences can then be observed.

Typical data for toggling measurements carried out using the double-axis Kerr system is shown in **Figure 13**. In accordance with what was discussed above, the two magnetic films which make up the free layer were balanced, giving no net moment at remanence. However,

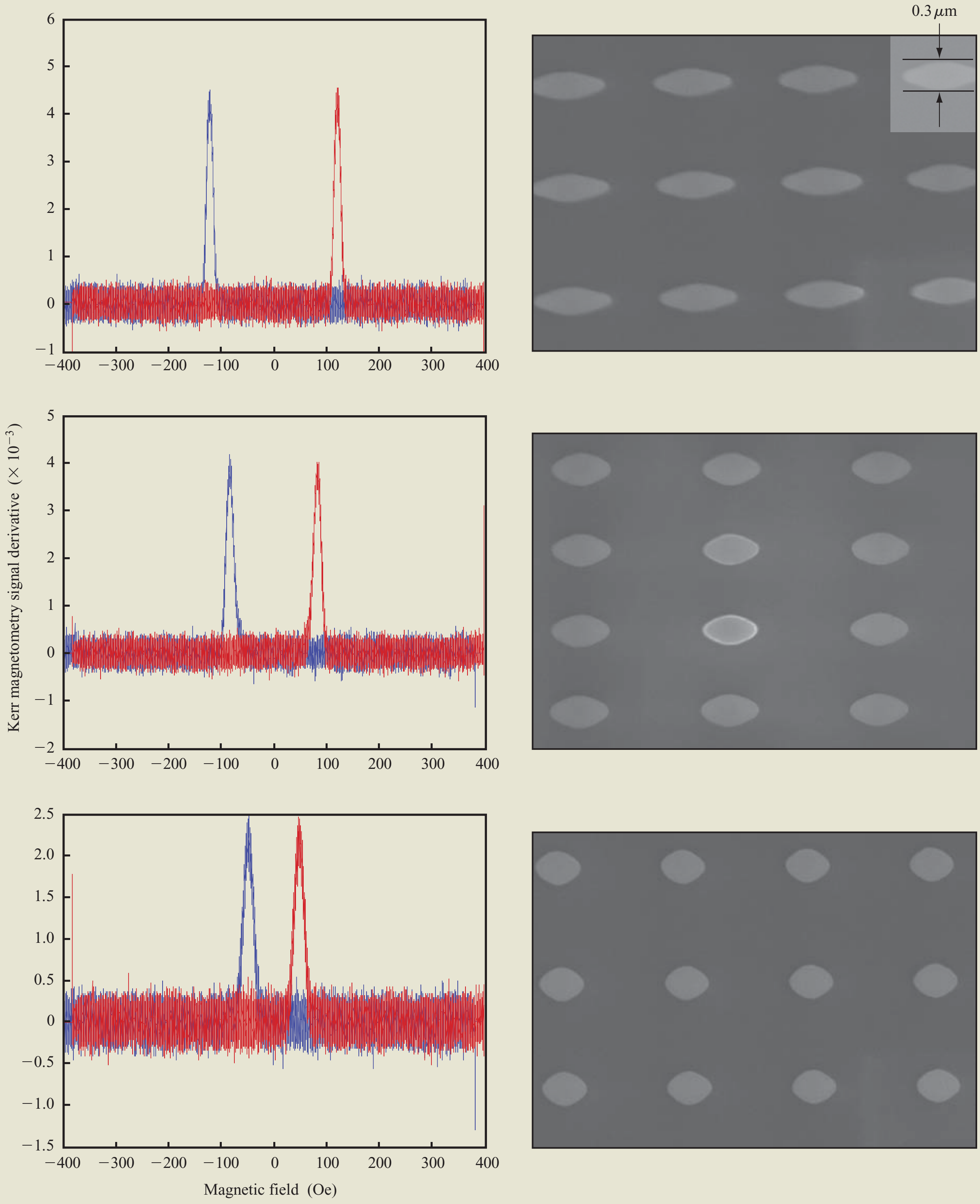

Figure 10

Illustrative Kerr measurements of switching field distributions for free-layer-only arrays of MTJs with a constant width of 0.3 μm and aspect ratios of 1.7, 2, and 2.5, respectively. Scanning electron micrographs of the arrays are shown to the right. Increasing the aspect ratio increases H_c and decreases its standard deviation; hence, AQF [defined as $H_c/s(H_c)$] rises rapidly with increasing aspect ratio.

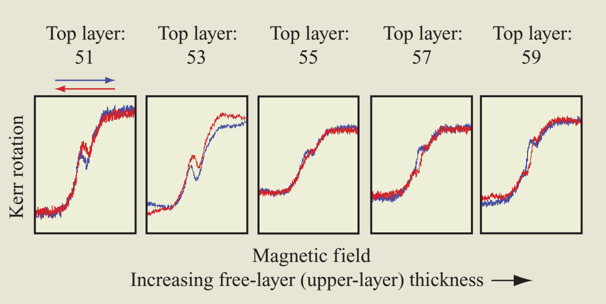

Figure 11

Illustrative swept Kerr magnetometry data for a series of 0.3-μm-diameter circular rotational-stack MTJs. The top magnetic free layer was increased in 2-Å steps. Examination of the hysteresis loops showed that the free layers were balanced for the center sample.

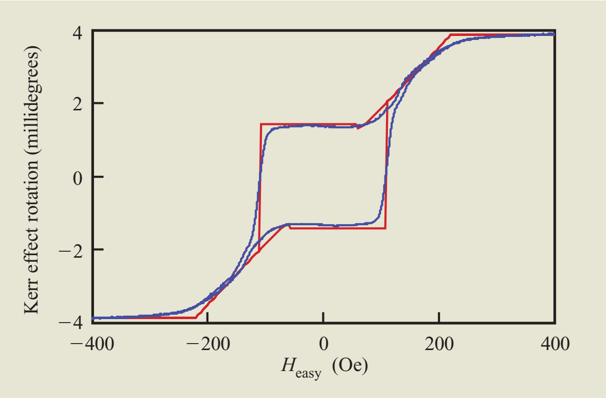

Figure 12

Illustrative one-axis Kerr magnetometry swept loops of array of 0.3-μm × 0.55-μm elliptical MTJs patterned from a rotational stack. Superimposed is the single-domain model prediction (in red) with a single fitting parameter to allow for attenuation of the portion of the Kerr effect signal due to light reflected from the buried-free-layer magnetic film.

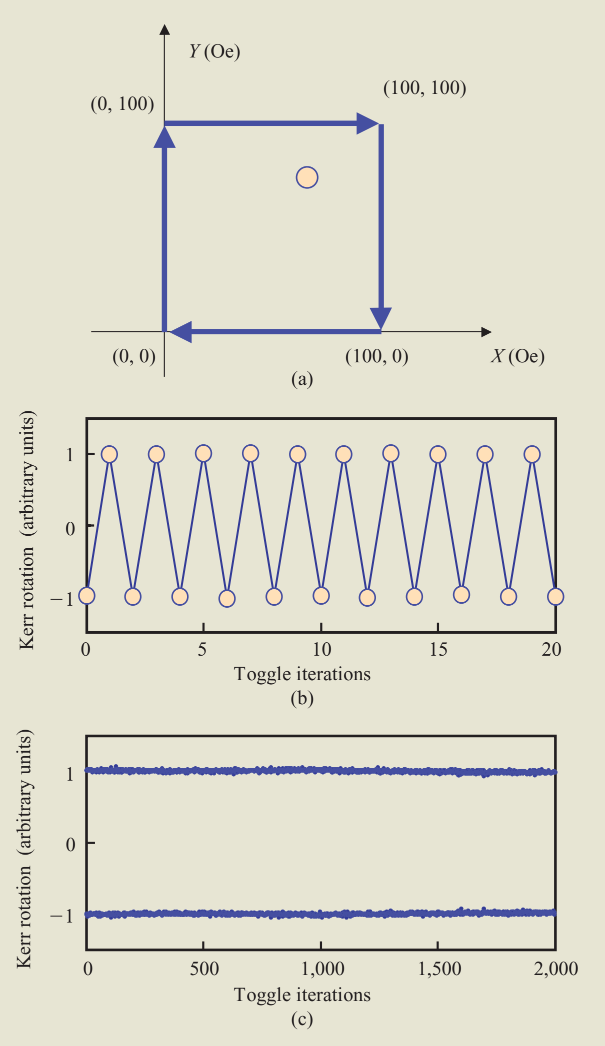

Figure 13

Typical toggle data obtained with double-axis Kerr magnetometry system: (a) Toggle field sequence applied to the sample with an external toroidal magnet. (b) Kerr magnetometry signal measured at zero field after each of 20 traversals of the toggle box, showing the two storage states which were sampled by the toggling procedure. (c) Sample switched repeatedly and consistently during the entire test, which lasted for more than 2,000 cycles.

a Kerr signal contrast was observed between the two toggle states of the MTJ due in large part to differences in the attenuation of light reaching the top and bottom magnetic films. The junctions were aligned with their easy axis at 45 degrees to the field axes of the tool. They were then subjected to a repeated magnetic field, applied in the form of toggle boxes. The boxes had a trajectory in the *xy* field plane, as illustrated in Figure 13(a). The magnetic field was applied to the sample in a square or box pattern, for which the following pair of values corresponded to word- and bit-line fields: (0 Oe, 0 Oe), (0 Oe, 100 Oe), (100 Oe, 100 Oe), (100 Oe, 0 Oe), (0 Oe, 0 Oe). The sample was placed in the tool in such a way that the toggle point (corresponding to the field box amplitude at which toggling first was observed) was (60, 60) at 45 degrees from the word lines and bit lines. After traversing each toggle box, the average remanent state of the junctions was measured [Figure 13(b)] and showed the characteristic toggle pattern. The junctions were found to toggle consistently after traversing more than 2,000 such boxes, as shown in Figure 13(c).

Concluding remarks

In this paper we have outlined characterization methods unique to MRAM and have shown how targeted measurements of magnetic and electrical properties of the basic MTJ device can provide leverage in the form of rapid feedback regarding materials and processing parameters. The methods in general are derived from existing methodologies but have been expanded or modified to fit the unique requirements of MRAM.

Acknowledgments

The authors thank Steve Brown for sample deposition and Eileen Galligan for measurements. Portions of this work were supported by DARPA under Contract No. MDA972-99C-009 and by the MRAM Development Alliance with Infineon.

References

1. S. S. P. Parkin, K. P. Roche, M. G. Samant, P. M. Rice, R. B. Beyers, R. E. Scheuerlein, E. J. O'Sullivan, S. L. Brown, J. Bucchignano, D. W. Abraham, Yu Lu, M. Rooks, P. L. Trouilloud, R. A. Wanner, and W. J. Gallagher, *J. Appl. Phys.* **85**, No. 8, 5828 (1999).
2. M. Durlam, P. Naji, A. Omair, M. M. DeHerrera, J. Calder, J. M. Slaughter, B. Engel, N. Rizzo, G. Grynkewich, B. Butcher, C. Tracy, K. Smith, K. Kyler, J. Ren, J. Molla, B. Feil, R. Williams, and S. Tehrani, *Digest of Technical Papers, IEEE International Symposium on VLSI Circuits* (Cat. No. 02CH37302), 2002, p. 158.
3. A. R. Sitaram, D. W. Abraham, C. Alof, D. Braun, S. Brown, G. Costrini, F. Findeis, M. Gaidis, E. Galligan, W. Glashauser, A. Gupta, H. Hoenigschmid, J. Hummel, S. Kanakasabapathy, I. Kasko, W. Kim, U. Klostermann, G. Y. Lee, R. Leuschner, K.-S. Low, Y. Lu, J. Nutzel, E. O'Sullivan, C. Park, W. Raberg, R. Robertazzi, C. Sarma, J. Schmid, P. L. Trouilloud, D. C. Worledge, G. Wright, W. J. Gallagher, and G. Muller, *Digest of Technical Papers, IEEE Symposium on VLSI Technology* (Cat. No. 03CH37407), 2003, p. 15.
4. M. Durlam, D. Addie, J. Akerman, B. Butcher, P. Brown, J. Chan, M. DeHerrera, B. N. Engel, B. Feil, G. Grynkewich, J. Janesky, M. Johnson, K. Kyler, J. Molla, J. Martin, K. Nagel, J. Nahas, J. Ren, N. D. Rizzo, T. Rodriguez, L. Savtchenko, J. Salter, J. M. Slaughter, K. Smith, J. J. Sun, M. Lien, K. Papworth, P. Shah, W. Qin, R. Williams, L. Wise, and S. Tehrani, *IEEE International Conference on Integrated Circuit Design and Technology* (Cat. No. 04EX866), 2004, p. 4559.
5. D. C. Worledge, *Appl. Phys. Lett.* **84**, No. 22, 4559 (2004).
6. See for example T. M. Maffitt, J. K. DeBrosse, J. A. Gabric, E. T. Gow, M. C. Lamorey, J. S. Parenteau, R. Willmott, M. A. Wood, and W. J. Gallagher, *IBM J. Res. & Dev.* **50**, No. 1, 25–39 (2006, this issue) and references cited therein.
7. D. Worledge, P. Trouilloud, D. W. Abraham, and J. Schmid, U.S. Patent 6,927,569, August 9, 2005.
8. D. C. Worledge and P. L. Trouilloud, *Appl. Phys. Lett.* **83**, No. 1, 84 (2003).
9. See *http://www.capres.com*.
10. D. C. Worledge, *Appl. Phys. Lett.* **84**, No. 10, 1695 (2004).
11. D. C. Worledge and D. W. Abraham, *Appl. Phys. Lett.* **82**, No. 25, 4522 (2003).
12. T. Uchihashi, Y. Fukano, Y. Sugawara, S. Morita, A. Nakano, T. Ida, and T. Okada, *Jpn. J. Appl. Phys. Part 2 (Lett.)* **33**, No. 11A, L1562 (1994).
13. H. Kubota, G. Reiss, H. Brückl, W. Schepper, J. Wecker, and G. Gieres, *Jpn. J. Appl. Phys. Part 2 (Lett.)* **41**, No. 2B, L180 (2002).
14. S. S. P. Parkin, C. Kaiser, A. Panchula, P. M. Rice, B. Hughes, M. Samant, and S.-H. Yang, *Nature Mater.* **3**, No. 12, 862 (2004).
15. M. Durlam, D. Addie, J. Akerman, B. Butcher, P. Brown, J. Chan, M. DeHerrera, B. N. Engel, B. Feil, G. Grynkewich, J. Janesky, M. Johnson, K. Kyler, J. Molla, J. Martin, K. Nagel, J. Ren, N. D. Rizzo, T. Rodriguez, L. Savtchenko, J. Salter, J. M. Slaughter, K. Smith, J. J. Sun, M. Lien, K. Papworth, P. Shah, W. Qin, R. Williams, L. Wise, and S. Tehrani, *Technical Digest. IEEE International Electron Devices Meeting*, 2003, p. 34.6.1.

Received April 24, 2005; accepted for publication May 25, 2005; Internet publication January 5, 2006

David W. Abraham *IBM Research Division, Thomas J. Watson Research Center, P.O. Box 218, Yorktown Heights, New York 10598 (dwabra@us.ibm.com)*. Dr. Abraham is a Research Staff Member in the Physical Sciences Department at the IBM Thomas J. Watson Research Center. He received a B.S. degree in physics from the University of Iowa in 1978, and M.S. and Ph.D. degrees in physics from Harvard University in 1979 and 1983, respectively. Following a three-year postdoctoral appointment at the University of California at Berkeley, where he worked on scanning tunneling microscopes, he joined IBM at the Thomas J. Watson Research Center. At IBM, he has worked on novel nanometer probe techniques based on scanning tunneling microscopy and atomic force microscopy, on a thermal imaging method for screening and analyzing disk drive surface defects, and, more recently, on the switching characteristics of MRAM tunnel junction devices.

Philip L. Trouilloud *IBM Research Division, Thomas J. Watson Research Center, P.O. Box 218, Yorktown Heights, New York 10598 (plt@us.ibm.com)*. Dr. Trouilloud is a Research Staff Member in the Physical Sciences Department at the IBM Thomas J. Watson Research Center. He is a graduate of the École Polytechnique, France. He completed his Doctorate at the Laboratoire de Physique des Solides in Orsay, France. After postdoctoral studies at the University of Texas at Austin, he joined the IBM Research Division in Yorktown Heights, New York. Dr. Trouilloud's work focuses on MRAM development, specifically on magnetic devices and magnetic test and characterization.

Daniel C. Worledge *IBM Research Division, Thomas J. Watson Research Center, P.O. Box 218, Yorktown Heights, New York 10598 (worledge@us.ibm.com)*. Dr. Worledge received a B.A. degree with a double major in physics and applied mathematics from the University of California at Berkeley in 1995. He received a Ph.D. degree in applied physics from Stanford University in 2000, with a thesis on spin-polarized tunneling in oxide ferromagnets. After joining the Physical Sciences Department at the IBM Thomas J. Watson Research Center as a postdoctoral researcher, he became a Research Staff Member in 2001, working on fast-turnaround measurement methods for magnetic tunnel junctions. In 2003, Dr. Worledge became the manager of the MRAM Materials and Devices group. His current research interests include magnetic devices and their behavior at small dimensions.